Korean J. Chem. Eng., 40(2), 369-378 (2023)
DOI: 10.1007/s11814-022-1307-9

pISSN: 0256-1115
eISSN: 1975-7220

Development of a liquid-based cytology method for detecting cervical cancer cells using functional gold nanorods

Eunseo Jeong*,‡, Jongjun Park*,‡, Hayoung Kim*, Sungjun Lee*,, Yonghyun Choi*,**, Masayoshi Tanaka***, and Jonghoon Choi*,**,†**

*School of Integrative Engineering, Chung-Ang University, Seoul 06974, Korea
**Feynman Institute of Technology, Nanomedicine Corporation, Seoul 06974, Korea
***Department of Chemical Science and Engineering, Tokyo Institute of Technology, 4259 Nagatsuta-cho, Midori-ku, Yokohama-shi, Kanagawa 226-8503, Japan
(*Received 12 July 2022 • Revised 27 September 2022 • Accepted 30 September 2022*)

Abstract−A cytopathology test for cervical cancer diagnosis has been introduced to complement the histopathology test. This study developed a new cervical cancer diagnostic method that complements the existing liquid cytology to reduce the diagnostician's skill dependence and to improve diagnostic accuracy. With the ease of introduction of surface functional groups and their high biocompatibility and stability, gold nanomaterials have been used to diagnose numerous biomolecules. CA125 and p16 markers were chosen as protein markers uniquely present in cervical cancer. Bioconjugation technology was used to form a stable bond between the target antibody and gold nanorods. Antibody-gold nanorods were administered to cervical cancer cells as a factor for optical microscopic analysis. The degree of cancer cell labeling was determined through additional fluorescence microscopy analysis. Additionally, a liquid-based cytology test mimicking the clinical environment was prepared, and the false-positive rate, false-negative rate, and accuracy were determined when the study strategy was implemented. The strategy validated in this study (antibody-gold nanorod-based cervical cancer diagnosis) suggests a method that can reduce the dependence on experts for the cancer cytology and can increase test accuracy.

Keywords: Cervical Cancer, Cytology, Gold Nanorod, CA125, p16, Cancer Diagnosis

INTRODUCTION

Cervical cancer is the second most prevalent malignancy among women worldwide [1]. More than 500,000 women are diagnosed each year with the disease, and more than 300,000 die [2]. Cervical cancer, therefore, necessitates early detection, as most cases are curable if detected and treated early [3]. Cervical cancer is caused by abnormal cell growth on the cervix lining. In its early stages, cervical cancer has few symptoms, so periodic screening is required [4,5]. Most cervical cancers are caused by infection with the high-risk strain of human papillomavirus (HPV) [1,6]. Although the recent development of a vaccine to prevent HPV infection has reduced the incidence of cervical cancer, the vaccine's high cost and logistical obstacles have hampered its widespread adoption [7]. In addition, since the current HPV vaccine does not cover all HPV virus infections but only types 16 and 18, a cervical cancer screening system that can accurately diagnose cervical cancer at an early stage is required [8-10].

The histopathological examination biopsy has historically been used for the diagnosis of cervical cancer. However, the economic and physical burdens placed on the patient are considerable for the test. In 1941, the Pap smear method was introduced as a cell pathology test [11,12] to compensate for the limitations mentioned above. In this technique, a cervical specimen is collected and smeared directly onto a glass slide, the stained slide is then examined under the microscope by a pathologist to diagnose cancer [13]. The liquid cervical cytology (LBC) method, which prevents cell degeneration, removes foreign substances, and smears only pure cells, is currently the most reliable method for diagnosing cervical cancer. A cervical sample is collected and placed in a vial containing a special reagent, and the cells are collected in the form of a suspension and spread a monolayer smear on a glass slide for testing [14,15]. The liquid cytology method, unlike the Pap smear, preserves cell shape so that cellular findings can be viewed in detail, and selection can be performed on a clean background by removing blood exudates and foreign substances [16,17]. However, this test method is highly dependent on the pathologist who conducts and interprets the test, and as a result, each pathologist makes a unique diagnosis [18,19].

Researchers are interested in gold nanoparticles due to their diverse properties and applications. They are used extensively in the diagnosis and treatment of cancer. Due to the optical properties of gold nanoparticles, which vary in color based on their size and shape and their low cytotoxicity, they are widely used in the diagnosis and treatment of cancer [20-23]. Additionally, as nanoparticles, they have a high surface-to-volume ratio, allowing for the attachment of numerous surface functional groups, and due to their nanoscale size, they can penetrate cells, allowing for processes such as cellular

†To whom correspondence should be addressed.
E-mail: nanomed@cau.ac.kr
‡These authors contributed equally.

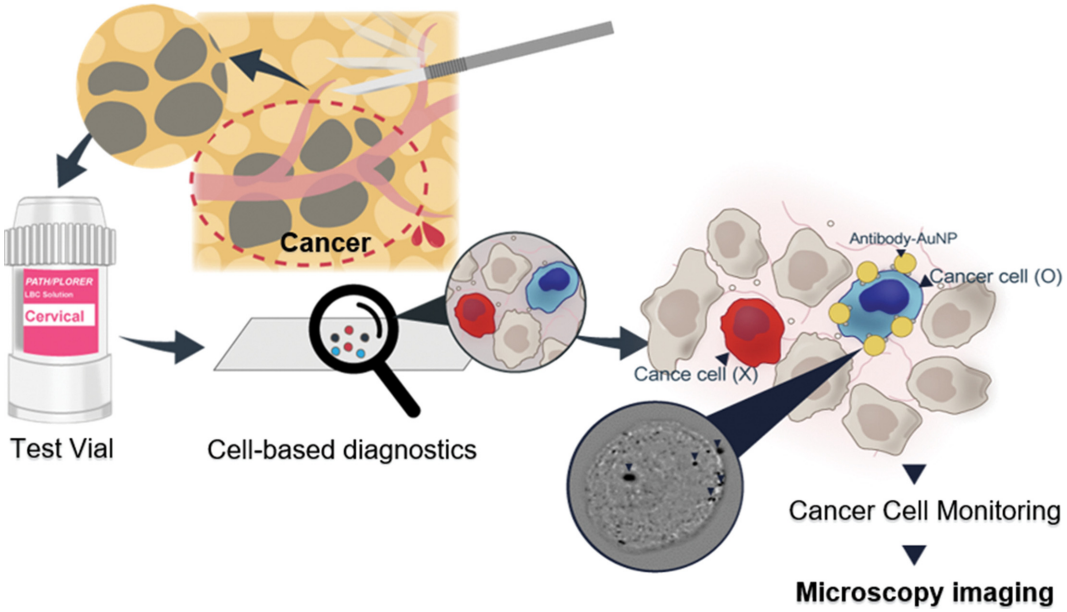

Fig. 1. Schematic of the current liquid cell test method and the diagnostic strategy presented in this study.

uptake [24,25]. Since the surface of gold nanoparticles has a strong affinity for the thiol moiety, they can be conjugated with various substances, including antibodies, ligands, and peptides, depending on their intended use. Particularly, numerous cancer-targeting technologies have been developed by conjugating antibodies to gold nanoparticles with diverse crosslinkers, such as EDC/NHS [26,27]. In this study, cervical cancer cells were captured by conjugating an antibody to gold nanorod, and the morphology of the nanorods was confirmed and analyzed using an optical microscope. Consequently, this study proposes a cervical cancer diagnosis strategy that optically identifies cancer cells through gold nanorods to which antibodies targeting markers uniquely present in cervical cancer cells are attached (Fig. 1).

CA125 and p16 were selected as markers present only in cervical cancer cells. CA125, also known as a cancer antigen, is a protein that is exclusively expressed in gynecological cancers such as cervical cancer, ovarian cancer, and endometrial cancer and is thus a well-established experimental and clinical marker for cervical cancer [28-32]. Recent papers have confirmed that CA125 exists as an endogenous membrane protein. In addition, researchers have determined that CA125 is present in the cell membrane in general and that it exists as an endogenous membrane protein [33].

The cell cycle regulatory protein p16INK4a (p16) hinders cell cycle progression by inhibiting cyclin-dependent kinases (CDKs) 4 and 6 [34]. Human papillomavirus infection (HPV) is strongly associated with cervical cancer incidence. By inhibiting the functions of cell cycle inhibitory proteins such as p53 and pRb, HPV E6, and E7 proteins promote progression from G1 to S phase. Glycolysis promotes cell proliferation, which in turn promotes cancer development [35]. In the process of HPV E7 protein binding to pRb and inactivating pRb function, p16INK4 is overexpressed due to negative feedback [36,37]. Multiple malignant tumors, including cervical cancer, malignant melanoma, gastrointestinal carcinoma, and lung cancer, have been linked to p16 protein overexpression [38-40].

As gold nanorods can be easily visualized under a microscope when attached to cells, the possibility of using cervical cancer cell specific antibody-gold nanorods as a supplementary LBC was investigated. By performing the antibody-gold nanorod-based cervical cancer diagnostic method in this manner, it is anticipated that this study will demonstrate improvement over conventional diagnostic methods, such as helping the increase of cervical cancer screening accuracy in LBC and the decreasing diagnostician dependence (Fig. 1).

MATERIALS AND METHODS

1. Materials

The HeLa and CaSki cervical cancer cell lines, as well as the CCD-986sk fibroblast cell line (CCD), were purchased from the Korean cell line bank. CaSki and CCD cell lines were cultured in Gibco RPMI Medium 1640 from Thermo Fisher (Massachusetts, U.S.A.).

Mucin 16, p16INK4a antibody was used in both the antibody screening experiment and the gold nanorod antibody. Alexa Fluor 488 Mucin 16 antibodies were supplied by Santa Cruz Bio Technology (Dallas, U.S.A.), while the p16 antibody (CDKN2A/p16INK4a Rabbit mAb) and fluorescent secondary antibody (FITC Goat Anti-Rabbit IgG) were purchased from Abclonal (Massachusetts, U.S.A.).

The selected antibody was conjugated with gold nanorods with diameters and lengths of 40 nm and 148 nm, respectively, purchased from Nanopartz (Colorado, U.S.A.). All chemicals used in the production of gold nanorods were used without further purification. Hexadecyltrimethylammonium bromide (CTAB>98%; NaOL >97%) and sodium oleate (NaOL>98%) were purchased from TCI America (Oregon, U.S.A.). Hydrogen tetracholoroaurate trihydrate ($HAuCl_4 \cdot 3H_2O$) was purchased from Acros Organics (New Jersey, U.S.A.). In addition, L-ascorbic acid (BioUltra>99.5%), silver nitrate

($AgNO_3$>99%), sodium borohydride ($NaBH_4$, 99%), oleylamine (technical grade, 70%), and hydrochloric acid (HCl, 37 wt% in water) were purchased from Sigma Aldrich (St. Louis, U.S.A.). NHS-PEG-SH was purchased from nanocs for carboxyl functionalization of gold nanorods to bind to antibodies. The process of treating the cells with gold nanorods conjugated with the antibody included fixation, permeabilization, blocking, and washing. As Fuji Film, 4% Paraformaldehyde Phosphate Buffer Solution (4% PFA) was used, and Triton X and Bovine Serum Albumin were purchased from Sigma Aldrich (St. Louis, U.S.A.), respectively. 1XPBS was acquired from Welgene (Gyeongsan, Korea).

In an experiment with mixed cell types, each cell was stained to distinguish between cancer cells and normal cells. Both Alexa Fluor 594 NHS Ester and Alexa Fluor 647 NHS Ester, manufactured by Thermo Fisher (Massachusetts, U.S.A.), were utilized at this time.

2. Gold Nanorod Synthesis and Antibody-gold-nanorod Binding Method

The 'seed-mediated growth method' [41] was utilized to produce gold nanorods. CTAB (5 mL, 0.2 M) and $HAuCl_4$ (2.5 mL, 1 mM) were combined with stirring, and then $NaBH_4$ (600 μL, 0.01 M) was added. At 30 °C, a seed solution was formed and briefly stirred when the color shifted from yellow to dark brown. Subsequently, to prepare a growth solution, 250 mL of tertiary distilled water was combined with 9 g of CTAB, 1.23 g of NaOL, and 24 mL of 4 mM $AgNO_3$. Following the addition of $HAuCl_4$ (250 mL, 1 mM), the mixture was kept for 15 min without stirring, followed by 90 min of stirring. Three milliliters of 37 wt% HCl was injected and stirred for 15 min. After adding ascorbic acid (1.25 mL, 64 mM), the solution was stirred until it was colorless. In addition, after injecting the seed solution (10 μL) and stirring for 30 seconds, the temperature was held at 30 °C for 12 h without stirring.

To functionalize the gold nanorods with carboxylic acid, HS-PEG-COOH was added to the gold nanorods produced using the aforementioned procedure and stirred. After that, 0.08% SDS-containing tertiary distillate water was added and stirred for one day. To remove unbound HS-PEG-COOH, the gold nanorods were centrifuged and redispersed in MES buffer with a pH of 5.5 twice. The EDC/NHS crosslinker was then added and stirred, followed by centrifugation and redispersion in MES buffer with a pH of 7. Antibody was injected and mixed for 24 h. The final antibody-gold nanorod conjugate was formed after centrifugation and redispersion in tertiary distilled water.

3. Antibody-gold Nanorod Treatment Test Method

Twenty-four hours was spent incubating cervical cancer cells HeLa and fibroblasts (normal control) CCD at 37 °C. The cells were then treated with a 2% paraformaldehyde solution and fixed for 20 min at 25 °C. Add 0.25% Triton X solution after fixation and proceed with 10 min of 25 °C permeabilization. Then, blocking was performed at 25 °C for 30 min using a 1% BSA (in PBS) solution. This procedure was performed to reduce non-specific binding between the gold nanorods and antibodies. Next, DAPI dye (1 μg/mL) was added and allowed to react at 25 °C for 5 min to stain the cell nucleus. Then, the antibody-gold nanorods were treated and reacted at 25 °C for 2 h. After treatment with a secondary antibody (FITC Goat Anti-Rabbit IgG) for subsequent fluorescence imaging, the mixture was reacted at 25 °C for 1 h. After the reaction was complete, optical and fluorescence microscopy were used for imaging.

Cervical cancer cells HeLa and fibroblasts (normal control) CCD were separated and fixed at 25 °C for 20 min with a 2% Paraformaldehyde solution to simulate the actual liquid cervical cancer test environment. To stain the cell membrane, cancer cells were treated with Alexa 647 dye (1 μg/mL), and normal cells were treated with Alexa 594 dye (1 μg/mL) for 15 min at 25 °C. The samples were then submerged in PATHPLORER Cervical Solution (20 mL) and stored at 4 °C for one day. The fixed cells were smeared onto slides using PATHPLORER PLUS 4.7, and a one-hour secondary fixation at 25 °C with 95% ethanol was performed. Then, blocking was performed at 25 °C for 30 min using a 1% BSA (in PBS) solution. This process was performed to reduce non-specific binding between the gold nanorods and antibodies. The antibody-gold nanorods were then treated and reacted for 2 h, and following treatment with a secondary antibody (FITC Goat Anti-Rabbit IgG) for subsequent fluorescence imaging, the reaction was carried out at 25 °C for 1 h. After the reaction was complete, optical and fluorescence microscopy were used for imaging.

4. Calculation of False-positive and False-negative Rates

4-1. Calculation of the False-positive Rate

Fibroblast (normal control) CCD was incubated at 37 °C for 24 h. After separating the cells, they were placed in 20 mL of PATHPLORER Cervical Solution and stored at 4 °C for one day. The fixed cells were smeared onto slides using PATHPLORER PLUS 4.7, and a 1-hour secondary fixation at 25 °C with 95% ethanol was performed. Then, blocking was performed at 25 °C for 30 min with a 1% BSA (in PBS) solution. This procedure was performed to reduce non-specific binding between the gold nanorods and antibodies. The antibody-gold nanorods were then treated and allowed to react for 2 h. After the reaction was complete, approximately 300 normal cells (CCD) were optically observed and analyzed. The number of normal cells bound to gold nanorods was compared to the total number of normal cells, and the false-positive rate was calculated using the formula below.

$$\text{False Positive (\%)} = \frac{\text{The number of CCD cells detected by GNR}}{\text{The number of total cells}} \times 100$$

4-2. Calculation of False-negative Rate

Cervical cancer cells HeLa and fibroblasts (normal control) CCD were incubated at 37 °C for 24 h. After each detachment, the cells were fixed for 20 min. Then, following fixation, cancer cells were treated with Alexa 647 dye (1 μg/mL), and normal cells were treated with Alexa 594 dye (1 μg/mL) and reacted at 25 °C to stain the cell membrane. Subsequently, after mixing at a specified ratio (HeLa : CCD=1 : 10) and immersion in PATHPLORER Cervical Solution (20 mL), the cells were fixed at 4 °C for 24 h. The fixed cells were smeared onto slides using PATHPLORER PLUS 4.7, and a 1-h secondary fixation at 25 °C with 95% ethanol was performed. Then, blocking was performed at 25 °C for 30 min using a 1% BSA (in PBS) solution. This procedure was performed to reduce non-specific binding between the gold nanorods and antibodies. The antibody-gold nanorods were then treated and reacted for 2 h, and following treatment with a secondary antibody (FITC Goat Anti-Rabbit IgG) for subsequent fluorescence imaging, the reaction was

carried out at 25 °C for 1 h. Through fluorescence and optical analysis, the detection accuracy and false-negative rate of gold nanorods were calculated as follows:

$$\text{False Negative (\%)} = \frac{\text{The number of HeLa cells undetected by GNR}}{\text{The number of HeLa cells}} \times 100$$

5. Evaluation of p16 Antibody-gold Nanorod Stability

An experiment was conducted to determine the degree to which the p16 antibody-gold nanorod conjugate maintains its stability during storage. The degree of labeling of cancer cells was evaluated immediately after synthesis, after 4 days, and after 30 days using the antibody-gold nanorod conjugate. Each test date compared and analyzed whether the antibody-gold nanorod conjugate could normally capture the p16 marker even after long-term storage and maintain cancer cell diagnosis accuracy. All antibody-gold nanorod conjugates were used in the experiment after being refrigerated at 4 °C, and the antibody concentration per 4×10^4 cells was diluted to 2.5 μg/mL. In addition, the analysis was conducted using the experimental method for determining the state of cell adhesion described previously.

RESULTS

1. Antibody Screening

CA125 and p16 markers were identified in cervical cancer cells. Subsequently, we measured the fluorescence expression level of the two markers via immunofluorescence staining using an antibody that targets them. To confirm the reaction between the marker and the antibody, HeLa, a cervical cancer cell, and CCD, a fibroblast, were introduced. Fluorescence was used to compare the interaction between the cell and the antibody following treatment with a target antibody and a secondary antibody to which a fluorescent dye specifically binding to the antibody was attached. CA125 is predominantly a membrane protein that has been implicated in cancer cell growth and epithelial cell defense. It protects cancer cells by forming a glycan-rich barrier and aids cancer cells in evading immune surveillance by inhibiting the NK cell activity. Since CA125 is a protein that is exclusively expressed in gynecological cancers such as cervical cancer, the level of expression of markers between each cell line can be confirmed by the binding of cervical cancer and normal cells to the anti-CA125 antibody. Similarly, p16 is a tumor suppressor protein that plays a significant role in cell circulation. However, p16 overexpression has been confirmed in many cancers, particularly cervical cancer. Cancer is closely associated with the p16 protein, which has multiple functions, including apoptosis, angiogenesis, and cell invasion. Since it has the potential to be used as a cervical cancer marker protein, it is possible to determine the expression level of the marker factor in each cell line by comparing the binding of cervical cancer and normal cells with the anti-p16 antibody. We used confocal fluorescence microscopy to determine the distribution of binding between each cell and anti-CA125 and anti-p16 antibodies (Fig. 2). According to the treated antibody, representative fluorescence images can be generated, and the antibody distribution around cells can be confirmed. The binding of anti-CA125 and anti-p16 antibodies to HeLa, a cervical cancer cell, exhibited a high level of green fluorescence. Also, it was

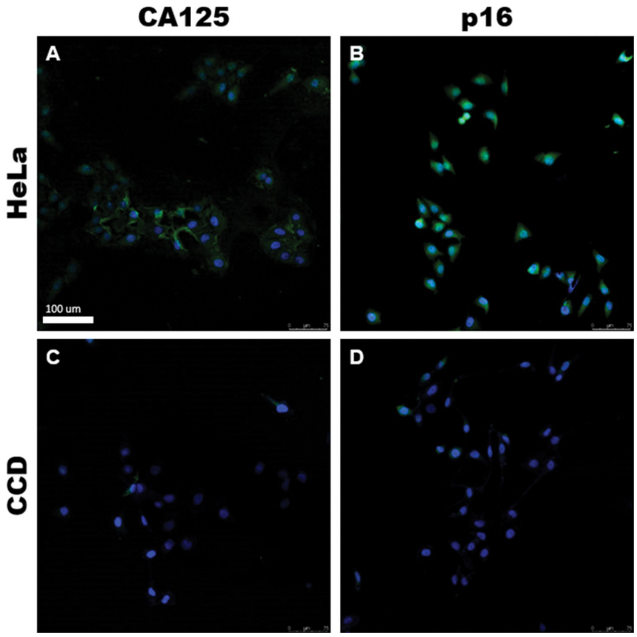

Fig. 2. Confirmation that CA125 and p16 antibodies bind to cells. (A-B) CA125 and p16 expression levels were measured in HeLa cells (cervical cancer cell line). (C-D) CA125 and p16 expression levels were evaluated in CCD cells (normal fibroblast cell line). (blue: nuclei, green (A, C): CA125, green (B, D): p16).

confirmed that anti-p16 antibodies showed slightly higher fluorescence than that of CA125. However, the binding of both antibodies to CCD cells used as a control was confirmed to be minimal. Therefore, anti-CA125 and anti-p16 antibodies were chosen for the treatment of cells with gold nanorods-conjugated antibodies.

2. Gold Nanorod Characterization

Measurements of absorbance, concentration, size distribution, and surface charge were used to characterize the synthesized gold nanorods. Absorbance was measured using a plate reader in the 300-900 nm wavelength range. Since the particles exhibited high absorbance at approximately 550 nm and 870 nm, it was determined that their aspect ratio was approximately 1 : 5. The particle concentration was approximately 2×10^{11} particles/mL, as measured by an NTA instrument. The particle size distribution and surface charge were analyzed using a DLS instrument. The size was approximately 25 nm along the minor axis, and 125 nm along the major axis, and the absorbance measurement confirmed that the result was consistent with the aspect ratio of 1 : 5. A positive surface charge was observed, and the CTAB used in the synthesis of gold nanorods was confirmed to coat the particles' periphery. In addition, transmission electron microscopy (TEM) was used to confirm that the gold nanorods had a rod-like shape. The above characterization confirmed that the gold nanorods that we synthesized were successfully formed. The gold nanorods were functionalized with carboxylic acid and then conjugated with an antibody-containing amine group using an HS-PEG-COOH crosslinker (Fig. 3).

3. Antibody-gold Nanorod Cell Treatment Experiment

The antibody-gold nanorod complex was applied to cervical cancer cell lines and normal cell lines for fluorescence and optical

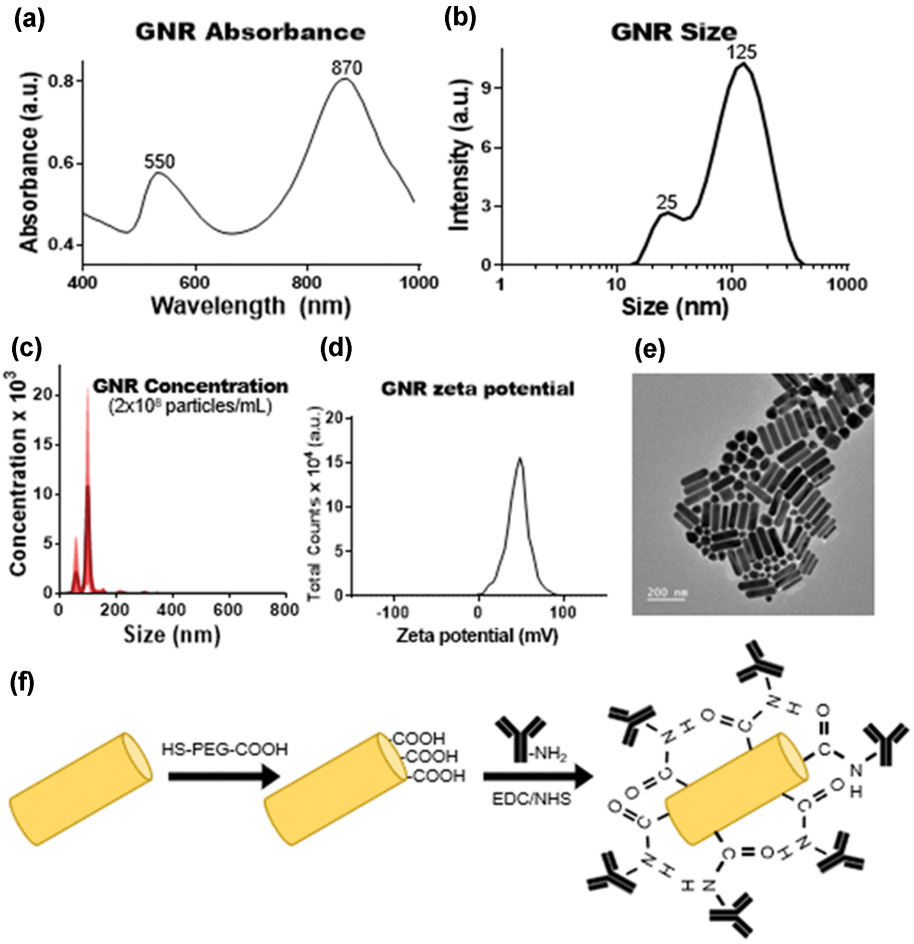

Fig. 3. (a) UV/visible graphs of the synthesized gold nanorod. Absorbance values were high in the wavelength bands of approximately 550 and 870 nm, indicating that the aspect ratio of the particles is approximately 1 : 5. (b) Size distribution of the synthesized gold nanorod; the short axis is approximately 25 nm, while the long axis is approximately 125 nm. (c) The concentration of the synthesized gold nanorods and 2×10^{11} particles/mL was present. (d) The surface charge of the synthesized gold. Due to the CTAB coating on the gold nanorods' surface, the positive surface charge of the particles was confirmed. (e) A TEM image of the synthesized gold nanorod. Taken at 1/10 the concentration of the final product. Even though it is not completely uniform, it can be confirmed that it has a rod-like shape. (f) A diagrammatic representation of antibody-gold nanorod conjugation. An antibody-gold nanorod conjugate was successfully formed by covalently bonding carboxylic acid-functionalized gold nanorod with an antibody-containing amine.

confirmation using a method similar to immunofluorescence staining. In the antibody-gold nanorod complex, the expression level of the fluorescent dye bound to the antibody was analyzed using a fluorescence microscope, and the degree of adhesion of the gold nanorods to the cells was confirmed using an optical microscope. Confirming the fluorescence expression level of cervical cancer cells using gold nanorods to which the anti-CA125 antibody and anti-p16 antibody were conjugated, it was determined that the fluorescence expression was greater in the cancer cell HeLa than in the normal cell CCD used as a control. Although normal cell lines expressed a low level of fluorescence, it was determined that cancer cells were overexpressed relative to cancer cell lines. As indicated by the fluorescence expression result, optical confirmation confirmed that the gold nanorods were specifically bound to the cancer cell line as opposed to the normal cell line (Fig. 4). As a result of confirming the specificity of the antibody-gold nanorod conjugate for cervical cancer, both markers demonstrated effective results with a significantly higher binding force level than normal cells. In the case of CA125, however, weak binding to the labeling factor was confirmed in cancer cells. This result was consistent with the previous result described in the section 3.1. Antibody screening. Therefore, it was determined that p16 had a greater degree of specificity for cervical cancer and was selected for further experiments.

In actual liquid cytology of the cervix, evaluation is performed on a suspended sample rather than an adherent cell. To simulate the actual test environment as closely as possible, an antibody-gold nanorod complex was treated, and optical confirmation was performed on cervical cancer cells suspended in a liquid.

After treatment with anti-p16 antibody-gold nanorods in floating cancer cells (HeLa), it was determined that the gold nanorods were attached to the cancer cell line's cells. To confirm the binding force of the gold nanorods, untreated cells served as a control and were compared using optical confirmation. As a result, a greater number of black spots were observed in cancer cells treated with

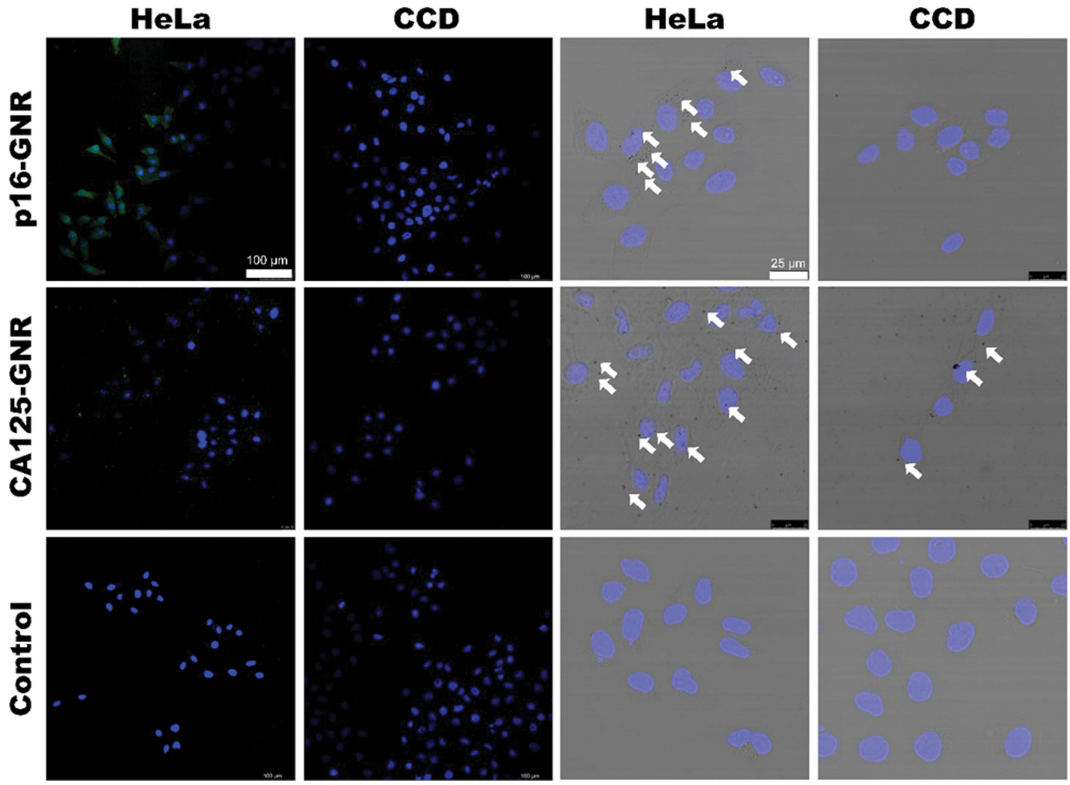

Fig. 4. Confirmation of cancer cell labeling based on fluorescence and light microscopy measurements. Green fluorescence is observed in cells expressing CA125 and p16 using Alexa 488 conjugated to the CA125 antibody and FITC conjugated to the p16 antibody, respectively. The presence of black gold nanorods indicates the degree of binding of antibody-gold nanorods to cells. (blue=nuclei, green=CA125, p16, and white arrow=gold nanorod).

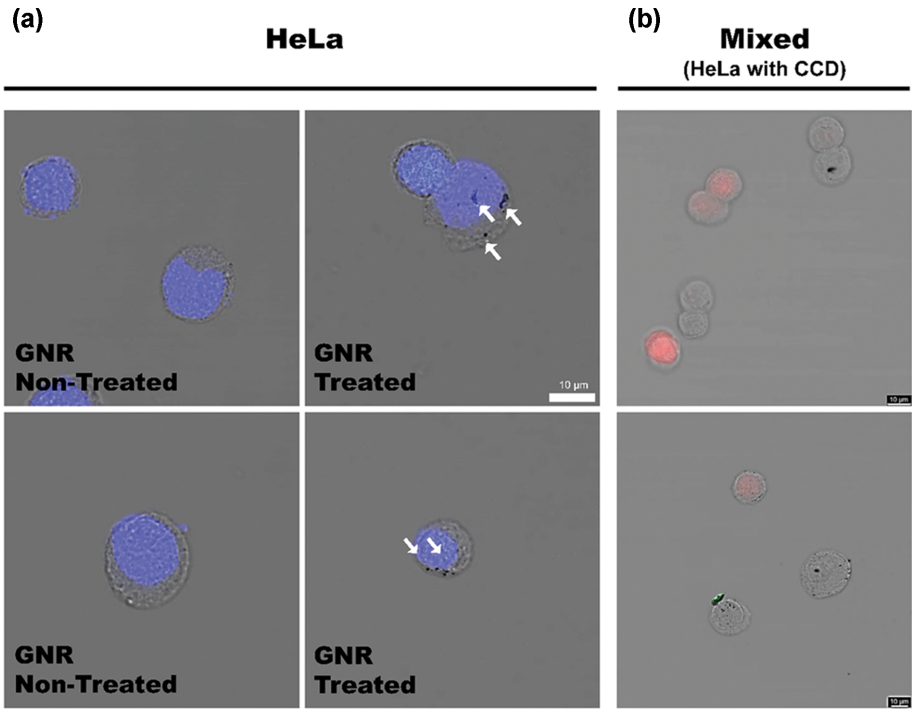

Fig. 5. (a) Confirmation of the degree of labeling of cancer cells (HeLa) as determined by fluorescence and optical microscopy. Cancer cells were either treated or untreated with gold nanorod. Cells treated with nanorod confirmed the specific binding of gold particles. (b) Verification of cancer cell labeling in a mixture of normal and malignant cells. The attachment of gold nanorods to unstained cancer cells has been confirmed. (blue represents nuclei, red represents CCD, and white represents a gold nanorod).

gold nanorods than in cancer cells not treated with gold nanorods, and it was confirmed that the gold nanorods were successfully bound to the cancer cells (Fig. 5(a)). Therefore, it was confirmed that the particles bind to cervical cancer cells specifically even when suspended.

In the actual test environment, cancer cells and normal cells are mixed with the sample, which is suspended. To simulate this clinical setting, a mixture of cervical cancer cell HeLa and normal cell CCD was tested, and the results were analyzed using fluorescence and optical microscopy. First, cervical cancer cells HeLa and normal cells CCD were cultured separately. Only the normal cells were stained with Alexa 594 dye and then mixed in a specific proportion. Fluorescence and light microscopy analysis confirmed that normal cells were successfully stained and that the two cell lines could be differentiated, and that the p16 Ab-gold nanorod conjugate labeled only unstained cervical cancer cells. Therefore, it was confirmed that the p16 Ab-gold nanorod conjugate was specifically tagged with cancer cells, even in the presence of normal and cancer cells (Fig. 5(b)).

4. Calculation of False-positive and False-negative Rates

As the study results confirmed that the p16 Ab-gold nanorods specifically labeled only cancer cells, false positives and negatives of the test method were determined. Due to the high false-positive rate of the current cervical cancer screening method, it is difficult to trust the test results. According to prior research, both the false-negative and positive rates are elevated [17,42-45]. By calculating the false-positive and false-negative rates of cancer cell detection evaluation using p16 antibody-gold nanorods, the effectiveness of the present technology for supplementing the conventional liquid cytology method and diagnosing cervical cancer was demon-

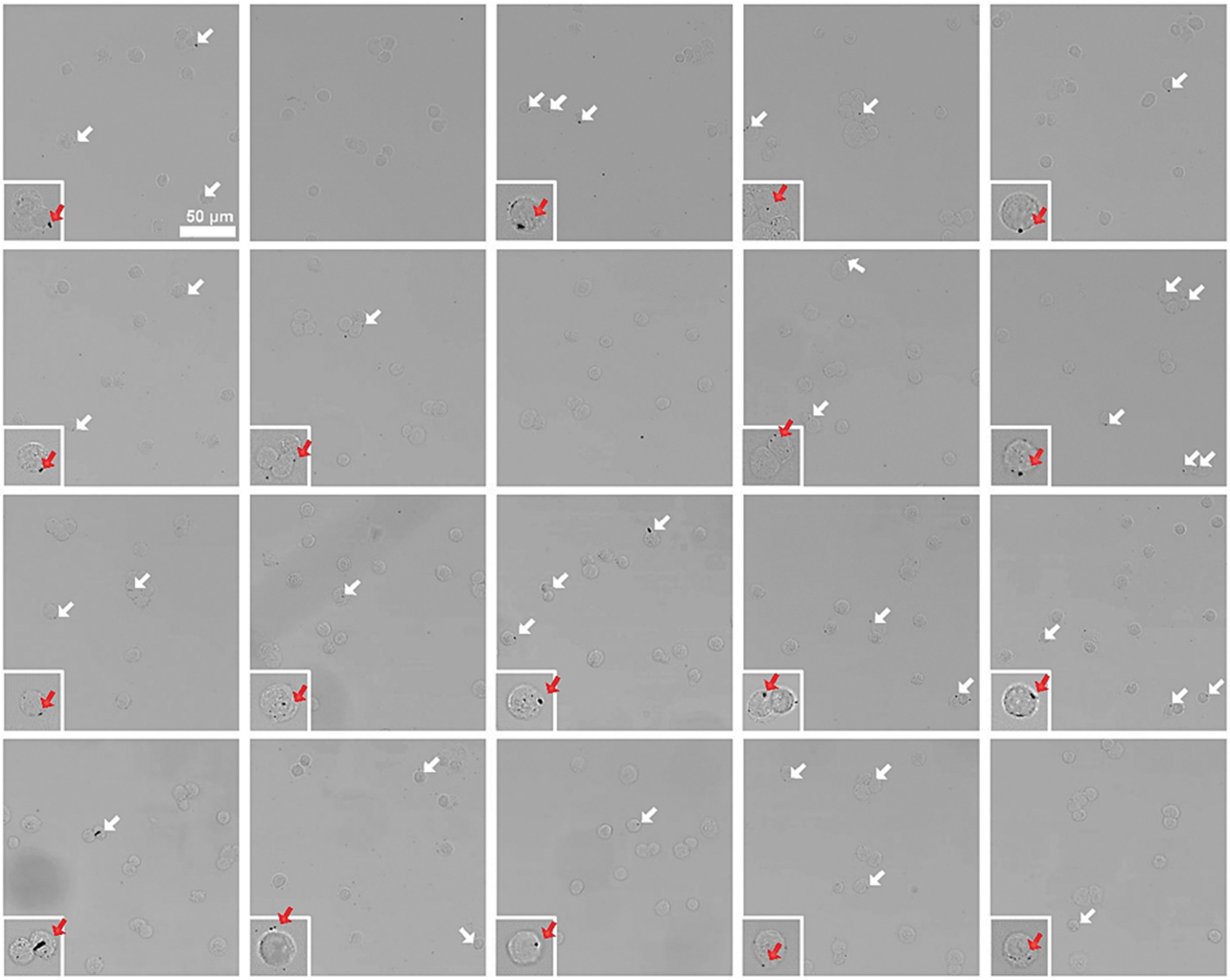

Fig. 6. Analysis of the percentage of false-positive normal cells. Confirmation of non-specific gold nanorod binding in normal cells (white arrow: gold nanorod).

Table 1. The number of CCDs in normal cells and CCDs bound to gold nanorods

CCD cells (Total: 304 cells)	13	13	16	21	18	14	15	12	13	13	15	21	16	13	17	18	14	15	13	14
GNR-CCD cells (Total: 38 cells)	3	0	3	2	1	5	2	0	1	2	2	1	3	2	3	1	2	1	3	1

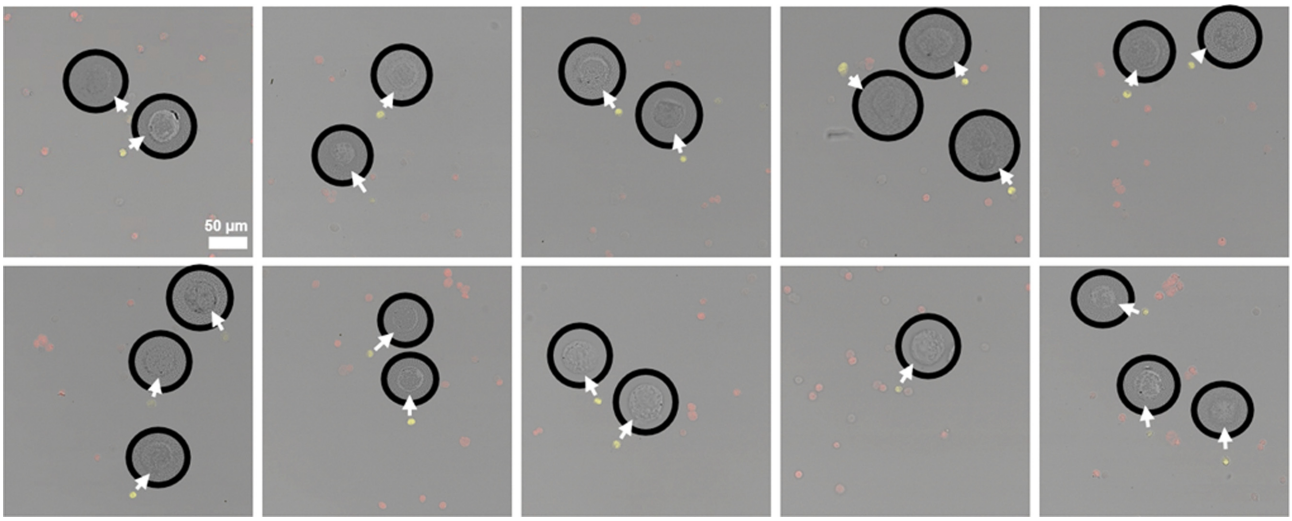

Fig. 7. The distribution of mixed cells (normal and cancer cells) and the degree of cancer cell labeling were checked using optical and fluorescence microscopy. The mixing ratio was approximately 1 : 10, which confirms that the gold nanorods selectively label only cancer cells (red=CCD, yellow=HeLa, and white arrow=HeLa cell enlargement).

Table 2. The total number of cells mixed with normal cells and cancer cells, the number of cancer cells, and the number of cancer cells combined with GNR

Total cells (Total: 245 cells)	17	24	16	24	13	12	16	14	25	25	11	12	17	21	20
HeLa cells (Total: 22 cells)	2	2	3	0	0	2	2	0	1	3	0	0	3	2	2
GNR-HeLa cells (Total: 18 cell)	2	1	3	0	0	2	1	0	0	3	0	0	3	1	2

strated.

Approximately 300 normal cells (CCD) were optically observed and analyzed, and the false-positive rate was calculated by comparing the number of gold nanorods-bound normal cells to the total number of normal cells (Fig. 6, Table 1). Because of the analysis, it was determined that approximately 12.5% of normal cells were incorrectly identified as cancerous (Number of total cells: 304; the number of normal cells bound to gold nanorods: 38). Consequently, the result was reduced compared to the false-positive rate of the existing liquid-based cell test.

Similarly, to calculate the false-negative rate in this study, normal and cancer cells were stained with various dyes. Approximately 300 cells were analyzed for fluorescence and optical properties, and the cell mixing ratio and false-negative rate were computed (Fig. 7). Cancer and normal cells were successfully stained using a fluorescence microscope, allowing the two cell lines to be distinguished. It was calculated to be approximately 1:11, confirming that the two cells were mixed normally. (Total number of cells: 267, number of normal cells: 245, number of cancer cells: 22) The false-negative rate was determined by comparing the number of cancer cells to which gold nanorods were not attached to the total number of cancer cells observed in the mixed cells (Table 2). The false-negative rate at which gold nanorods were unable to detect cancer cells was calculated to be 18.2% based on 55 analyses (Total number of cancer cells: 22, unbound cancer cells: 4). Consequently, the false-negative rate was reduced compared to the existing liquid-based cell test. In addition, the detection accuracy of the gold nanorods was determined by comparing the number of cancer cells to which the nanorods were bound to the total number of cancer cells observed in the mixed cells. The analysis determined that the gold nanorods' accuracy was approximately 81.8% (the total number of cancer cells: 22, the number of cancer cells bound to the gold nanorods: 18). Therefore, improved results were confirmed compared to the accuracy of the existing liquid cytometry method [17, 46].

The aforementioned study results confirmed that the cervical cancer diagnostic method presented in this study has lower false-negative and false-positive rates and greater accuracy than the conventional cervical cancer diagnostic method, uterine biopsy. Thus, it is possible to confirm the utility and efficacy of this diagnostic method for overcoming the limitations of the current cervical cancer screening by enhancing the cancer detection potential and accuracy of the strategy using the p16 Ab-gold nanorod.

5. Antibody-gold Nanorod Stability Evaluation

An experiment was conducted to determine the degree to which the p16 antibody-gold nanorod conjugate maintains its stability during storage. Fluorescence imaging confirmed that cervical cancer cells overexpressed fluorescence immediately after synthesis, after 4 days, and after 30 days. CCD, a normal cell line, exhibited no fluorescence immediately after synthesis, 4 days after synthesis, and 30 days after synthesis, whereas HeLa, a cervical cancer cell, exhibited a greater degree of fluorescence expression than the normal cell line. By day 30, optical confirmation revealed that all of them had successfully bound to cancer cells. As indicated by the fluorescence imaging results, all normal cell lines did not bind to gold nanorods until day 30, whereas cancer cell lines displayed a

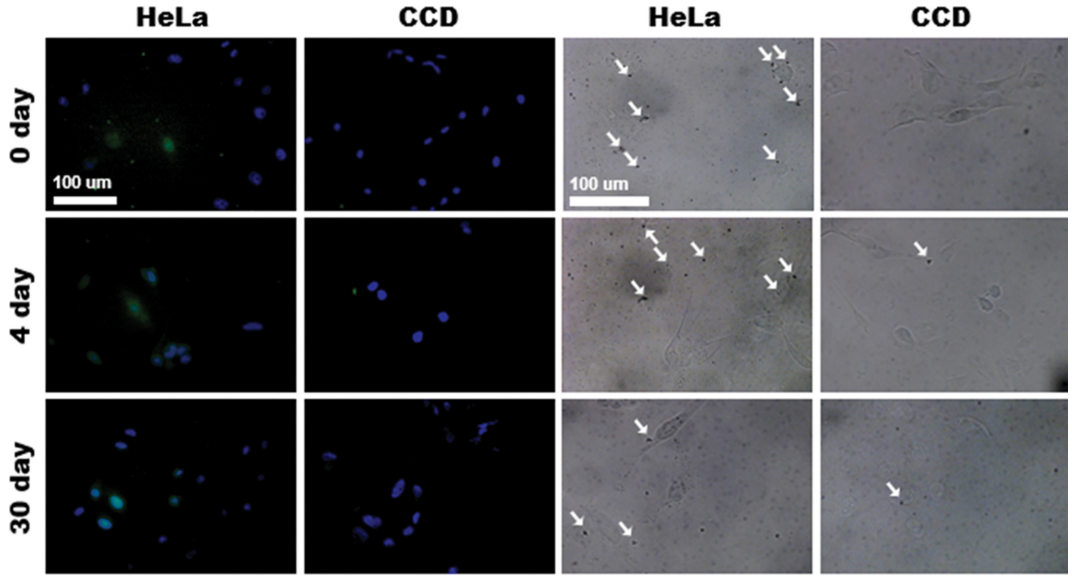

Fig. 8. Confirmation of cancer cell labeling based on fluorescence and light microscopy measurements. As a result of the measurement, identical fluorescence expression levels and adhesion of gold nanorods were observed from the moment of synthesis to 30 days later. Therefore, it was confirmed that the conjugate of antibody and gold nanorods was stable for up to 30 days.

high affinity (Fig. 8). Consequently, it was confirmed that the antibody-gold nanorod conjugate was stable for 30 days.

DISCUSSION

Due to the high cure rate of cervical cancer resulting from early detection, it is crucial to ensure the accuracy and timeliness of diagnosis [5,47]. The current LBC is dependent on the expertise of the pathologist, has limitations in its effectiveness and efficiency, and it is necessary to supplement its accuracy due to false positives and negatives that might have been dependent on the pathologists [18, 19]. This study proposes a new strategy that enables reliable cervical cancer diagnosis using antibody-gold nanorod conjugates in an effort to reduce the reliance on the skill of the pathologists performing the LBC and improve the diagnostic accuracy. By introducing an antibody that specifically labels a protein found in cervical cancer, the false-positive rate was minimized, which was visualized through the optical properties of gold nanorods. In addition, by introducing a secondary antibody with a fluorescent dye attached, the degree of cancer cell labeling was evaluated via fluorescence and optical microscopy.

CONCLUSION

As a result of this study, it was confirmed that cancer marker targeting can improve the accuracy of a cervical cancer diagnosis. The degree of cervical cancer labeled was optically verified using gold nanorods. Through bioconjugation technology, a stable conjugate was produced with the antibody. Then, using optical and fluorescence microscopy, it was possible to successfully design a diagnostic method that detects cancer cells but not normal skin cells or normal cervical cells. The combination of a gold nanorod-based carrier and an antibody, a cancer cell marker, confirmed that the antibody-gold nanorod-based cervical cancer diagnostic strategy presented in this study may help supplement the effectiveness of current LBC.

ACKNOWLEDGEMENTS

This research was supported by the Chung-Ang University Research Grant in 2021. This work was also supported by the National Research Foundation of Korea (NRF) grant funded by the Korean government (MSIT) (No. 2020R1A5A1018052). This work was also supported by the Korea Environment Industry & Technology Institute (KEITI) funded by the Korea Ministry of Environment (MOE) (No. 2022002980003).

AUTHOR CONTRIBUTIONS

Jonghoon Choi supervised the study. Eunseo Jeong, Jongjun Park, Hayoung Kim and Yonghyun Choi designed the study and performed the experiments. Eunseo Jeong, Jongjun Park, Hayoung Kim, and Sungjun Lee participated in the experiments. Eunseo Jeong, Jongjun Park and Yonghyun Choi performed data analyses. Eunseo Jeong, Jongjun Park, Masayoshi Tanaka and Jonghoon Choi wrote the manuscript.

COMPETING INTERESTS

The authors declare no competing interests.

REFERENCES

1. S. E. Waggoner, *Lancet*, **361**, 9376 (2003).
2. F. Bray, J. Ferlay, I. Soerjomataram, R. L. Siegel, L. A. Torre and A. Jemal, *CA: A Cancer J. Clinicians*, **68**, 6 (2018).

3. P. A. Cohen, A. Jhingran, A. Oaknin and L. Denny, *Lancet*, **393**, 10167 (2019).
4. A. Duenas-Gonzalez, M. Lizano, M. Candelaria, L. Cetina, C. Arce and E. Cervera, *Mol. Cancer*, **4**, 1 (2005).
5. T. A. Kessler, S*emin Oncol Nurs*., **33**, 2 (2017).
6. S. Dasari, R. Wudayagiri and L. Valluru, *Clin. Chim. Acta*, **445**, 7 (2015).
7. V. Madrid-Marina, K. Torres-Poveda, G. Lopez-Toledo and A. Garcia-Carranca, *Arch. Med. Res*., **40**, 6 (2009).
8. D. M. Harper, E. L. Franco, C. Wheeler, D. G. Ferris, D. Jenkins, A. Schuind, T. Zahaf, B. Innis, P. Naud, N. S. De Carvalho, C. M. Roteli-Martins, J. Teixeira, M. M. Blatter, A. P. Korn, W. Quint, G. Dubin and H. P. V. V. S. G. GlaxoSmithKline, *Lancet*, **364**, 9447 (2004).
9. L. A. Koutsky, K. A. Ault, C. M. Wheeler, D. R. Brown, E. Barr, F. B. Alvarez, L. M. Chiacchierini and K. U. Jansen, *N. Engl. J. Med*., **347**, 1645 (2002).
10. N. Wentzensen, M. E. Sherman, M. Schiffman and S. S. Wang, *Gynecol Oncol*., **112**, 293 (2009).
11. H. M. Shingleton, R. L. Patrick, W. W. Johnston and R. A. Smith, *CA Cancer J. Clin*., **45**, 5 (1995).
12. G. N. Papanicolaou and H. F. Traut, *Arch. Pathol. Lab. Med*., **121**, 3 (1997).
13. M. S. Khan, F. Y. Raja, G. Ishfaq, F. Tahir, F. Subhan, B. M. Kazi and K. A. Karamat, *Pak. J. Med. Res*., **44**, 111 (2005).
14. H. S. Cronje, *Int. J. Gynaecol Obstet*., **84**, 101 (2004).
15. R. K. Gibb and M. G. Martens, *Rev. Obstet. Gynecol*., **4**, S2 (2011).
16. C. Gabriel, R. Achten and M. Drijkoningen, *Acta Cytol*., **48**, 6 (2004).
17. U. Singh, S. Qureshi, N. Negi, N. Singh, M. Goel and K. Srivastava, *Ind. J. Med. Res*., **147**, 3 (2018).
18. J. Jin and C.-Y. Yue, *J. Lab. Med*., **44**, 3 (2020).
19. E. W. de Bekker-Grob, I. M. de Kok, J. Bulten, J. van Rosmalen, J. E. Vedder, M. Arbyn, P. J. Klinkhamer, A. G. Siebers and M. van Ballegooijen, *Cancer Causes Control*, **23**, 8 (2012).
20. L. Dykman and N. Khlebtsov, *Chem. Soc. Rev*., **41**, 6 (2012).
21. E. C. Dreaden, A. M. Alkilany, X. Huang, C. J. Murphy and M. A. El-Sayed, *Chem. Soc. Rev*., **41**, 7 (2012).
22. E. Boisselier and D. Astruc, *Chem. Soc. Rev*., **38**, 6 (2009).
23. R. J. Newhouse and J. Z. Zhang, *Reviews in Plasmonics 2010*, Springer Nature, Switzerland (2012).
24. R. Mout, D. F. Moyano, S. Rana and V. M. Rotello, *Chem. Soc. Rev*., **41**, 7 (2012).
25. L. A. Dykman and N. G. Khlebtsov, *Chem. Rev*., **114**, 2 (2014).
26. T. Burgi, *Nanoscale*, **7**, 38 (2015).
27. M. H. Jazayeri, H. Amani, A. A. Pourfatollah, H. Pazoki-Toroudi and B. Sedighimoghaddam, *Sensing and Bio-sensing Research*, **9**, 17 (2016).
28. G. L. Goldberg, A. Sklar, K. A. O'Hanlan, P. A. Levine and C. D. Runowicz, *Gynecol Oncol*., **40**, 3 (1991).
29. H. Shen, M. Guo, L. Wang and X. Cui, *Genes Genomics*, **42**, 2 (2020).
30. D. P. Bender, J. I. Sorosky, R. E. Buller and A. K. Sood, *Am. J. Obstet. Gynecol*., **189**, 1 (2003).
31. M. Porika, A. K. Vemunoori, R. Tippani, A. Mohammad, S. R. Bollam and S. Abbagani, *Asian Pac. J. Cancer Prev*., **11**, 6 (2010).
32. L. L. Zhou, Y. Shen, J. M. Gong, P. Sun and J. H. Sheng, *Oncotarget*, **8**, 41 (2017).
33. A. Crawford, L. Haber, M. P. Kelly, K. Vazzana, L. Canova, P. Ram, A. Pawashe, J. Finney, S. Jalal, D. Chiu, C. A. Colleton, E. Garnova, S. Makonnen, C. Hickey, P. Krueger, F. DelFino, T. Potocky, J. Kuhnert, S. Godin, M. W. Retter, P. Duramad, D. MacDonald, W. C. Olson, J. Fairhurst, T. Huang, J. Martin, J. C. Lin, E. Smith, G. Thurston and J. R. Kirshner, *Sci. Transl. Med*., **11**, 497 (2019).
34. J. Roelens, M. Reuschenbach, M. von Knebel Doeberitz, N. Wentzensen, C. Bergeron and M. Arbyn, *Cancer Cytopathol*., **120**, 5 (2012).
35. C. Romagosa, S. Simonetti, L. Lopez-Vicente, A. Mazo, M. E. Lleonart, J. Castellvi and S. Ramon y Cajal, *Oncogene*, **30**, 18 (2011).
36. K. Munger, B. A. Werness, N. Dyson, W. C. Phelps, E. Harlow and P. M. Howley, *EMBO J*., **8**, 13 (1989).
37. M. Reuschenbach, T. Waterboer, K. L. Wallin, J. Einenkel, J. Dillner, E. Hamsikova, D. Eschenbach, H. Zimmer, B. Heilig, J. Kopitz, M. Pawlita, M. Doeberitz and N. Wentzensen, *Int. J. Cancer*, **123**, 11 (2008).
38. F. Haller, A. Agaimy, S. Cameron, M. Beyer, B. Gunawan, N. Happel, C. Langer, G. Ramadori, A. von Heydebreck and L. Fuzesi, *Histopathology*, **56**, 3 (2010).
39. K. Bastide, M. N. Guilly, J. F. Bernaudin, C. Joubert, B. Lectard, C. Levalois, B. Malfoy and S. Chevillard, *Lung Cancer*, **63**, 3 (2009).
40. M. Schwabe and M. Lubbert, *Curr. Pharm. Biotechnol*., **8**, 6 (2007).
41. X. Ye, C. Zheng, J. Chen, Y. Gao and C. B. Murray, *Nano Lett*., **13**, 2 (2013).
42. J. Monsonego, M. G. Hudgens, L. Zerat, J. C. Zerat, K. Syrjanen, P. Halfon, F. Ruiz and J. S. Smith, *Int. J. Cancer*, **129**, 3 (2011).
43. B. Kirschner, K. Simonsen and J. Junge, *Cytopathology*, **17**, 4 (2006).
44. H. W. Kaufman, D. P. Alagia, Z. Chen, A. Onisko and R. M. Austin, *Am. J. Clin. Pathol*., **154**, 4 (2020).
45. J. Tanabodee, K. Thepsuwan, A. Karalak, O. Laoaree, A. Krachang, K. Manmatt and N. Anontwatanawong, *Asian Pac. J. Cancer Prev*., **16**, 16 (2015).
46. H. Ikenberg, C. Bergeron, D. Schmidt, H. Griesser, F. Alameda, C. Angeloni, J. Bogers, R. Dachez, K. Denton, J. Hariri, T. Keller, M. von Knebel Doeberitz, H. H. Neumann, L. M. Puig-Tintore, M. Sideri, S. Rehm, R. Ridder and P. S. Group, *J. Natl. Cancer Inst*., **105**, 20 (2013).
47. G. A. Mishra, S. A. Pimple and S. S. Shastri, *Ind. J. Med. Paediatr. Oncol*., **32**, 3 (2011).